Int J Adv Manuf Technol (2015) 80:625–635
DOI 10.1007/s00170-014-6378-2

ORIGINAL ARTICLE

Material removal profile for large mould polishing with coated abrasives

Guilian Wang · Xiaoqin Zhou · Xu Yang · Haibo Zhou · Guangjun Chen

Received: 5 March 2014 / Accepted: 8 September 2014 / Published online: 1 April 2015

Abstract This paper analytically develops a type of model for predicting material removal depth in large mould polishing with coated abrasives. This model based on the statistical theory, and the abrasive material surface contact mechanics is established. The material removal depth is calculated by integrating the linear removal intensity or the removal depth per unit time along the polishing path. The material removal depth profiles of the circular abrasive tool and the annular abrasive tool are presented when polishing paths are a straight line and a curve, respectively. The effects of process parameters on the material removal depth are simulated and analyzed, such as polishing pressure, feed rate, tool speed, and internal radius, when the polishing path is a straight line. The workpiece surfaces after milling were polished by using annular abrasive tool moving along a straight line in the experiment. This model is evaluated by comparing the theoretical material removal depth with those experimental results available. It is concluded that the experiment results are approximately consistent with the model predictions.

Keywords Polishing · Material removal profile · Mould · Coated abrasives

Nomenclature

d_m	Maximum diameter of the abrasive grains (*mm*)
d_{max}	Minimum diameter of the abrasive grains (*mm*)
d_{min}	Mean diameter of the abrasive grains (*mm*)
dt	Time interval
dx,dy	Components of infinitesimal M
dz	Depth of material removal at infinitesimal M during the time interval dt (*mm*)
E^*	Contact modulus of the abrasive grain and workpiece (*MPa*)
E_1, E_2	Young's modulus of the abrasive grain and workpiece (*MPa*)
D_l	Linear removal intensity, a non-dimensional number
D_t	Material removal depth of unit time (mm/min)
h	Abrasive grain protrusion height (*mm*)
$f(h)$	Gaussian distribution function, a non-dimensional number
F	Polishing force (*N*)
H_B	Brinell hardness of the workpiece surface (N/mm^2)
k	Ratio of the cutting depth to the indentation depth, a non-dimensional number
L_1,L_2	Start point and end point of the polishing contact path
m	Indentation depth of the abrasive grain (*mm*)
M	Infinitesimal part in the workpiece surface
N_0	Number of the abrasive grains per unit area ($grains/mm^2$)
n_s	Angular velocity of tool rotation (r/min)
R	Curvature radius (mm)
R_0	The curvature radius of curve (mm)
R_1	Radius of the circle abrasive tool (mm)
R_2	Inner circle radius of the annular abrasive tool (mm)
S	Structure number of the abrasive tool, a non-dimensional number
t_1,t_2	Start time and end time of the polishing contact path
v	The relative velocity between the tool and the workpiece (*mm*/min)

G. Wang (✉) · H. Zhou · G. Chen
College of Mechanical Engineering, Jiamusi University, Jiamusi 154007, People's Republic of China
e-mail: wangguilian@gmail.com

X. Zhou · X. Yang
College of Mechanical Engineering, Jilin University, Changchun 130025, China

v_a	Feed rate (*mm*/min)
v_s	The tool rotation speed of A point (*mm*/min)
v_1, v_2	Poisson's ratio of the abrasive grain and workpiece, a non-dimensional number
V_g	Grain ratio (%)
y_1,y_2	Start point and end point of the polishing contact path
Z_M	The material removal depth for position M (mm)
$Z(x)$	Material removal depth function (mm)

Greek letters

α	Apical angle (°)
$\delta_{\max}$	Maximum overlap of elastic contact (mm)
θ	Included angle between tool rotation speed direction and feed rate direction (°)
θ_2	Angle of end position of polishing contact trajectory (°)
θ_4	Angle of start position of polishing contact trajectory (°)
σ	Standard deviation of Gaussian distribution (mm)
ω	Angular velocity of tool rotation (rad/minute)
ω_{o1}	The angle velocity of tool along curve movement direction (rad/minute)

1 Introduction

With the development of automobile industry, aeronautics and astronautics industry, high quality and low-cost manufacture technology for large mould have been widely concerned by researchers, among which mechanical polishing using coated abrasives is a key step in large mould finishing process. The automatic polishing systems used for finishing large mould surface have been developed in these years [1]. It is very important how to efficiently control machining parameters to realize the uniform material removal process under various conditions. The material removal profile of workpiece surface can give an indication of the uniformity of material removal, which can be obtained in terms of the material removal depth of various position of workpiece surface. So, it is obviously essential to study and model the material removal depth, which has been a subject of intensive research in recent years.

Many researchers have already done much work about the material removal mechanisms and uniform material removal control for these years, which can provide insights into how basic process parameters influence material removal rates [2]. At present, the material removal models about mould polishing can be generally classified into four categories as follows:

The first approach is based on Preston hypothesis [3–8]. It refers that the material removal depth per time is directly proportional to polishing pressure and instantaneous velocity. In this hypothesis, other factors except velocity and pressure are regarded as a proportional constant, such as surface roughness, workpiece material type, and the abrasive tool. At present, many material removal models are based on Preston equation such as mould surface polishing, chemical mechanical polishing, and optical surface polishing controlled by computer. Guo et al. proposed the material removal rate model based on Preston's equation in ultra-fine polishing of optical glass with magnetic compound fluid slurry and investigated the effects of pressure and shear stress on material removal rate [3]. According to Preston's equation, Guo et al. modeled the material removal depth for a kind of novel vibration-assisted polishing system used for finishing high precision mould producing the micro-optical lenses [5]. Liu et al. presented a comprehensive model for the copper material removal in a chemical mechanical polishing process in which both chemical and mechanical effects are taken into consideration [6]. According to Preston's law, Cheung et al. established the integrated material removal rate in structure surface generation using computer-controlled ultra-precision polishing [8]. However, Preston's equation is only an empirical hypothesis and for lack of accurate theory, so it must be revised according to the machining conditions in practice.

The second approach makes use of the statistical theory, the contact elastic mechanics, the contact plastic mechanics, and the abrasive cutting theory [9–15]. Assuming further that the heights of pad asperities are exponentially distributed in chemical mechanical polishing, Kim et al. established contact mechanics models and analyzed the effect of pad-asperity curvature on material removal rate and found that the material removal rate can be improved by increasing the ratio of asperity radius and the standard deviation of asperity heights [9]. Lin and Wang proposed a new theoretical model for abrasive removal depth for polishing a sapphire wafer using chemical mechanical polishing with a polishing pad [10]. Lee et al. developed a novel semi-empirical material removal rate model [11]. This model incorporates the effects of particle size, particle concentration, slurry flow rate, area density of the pad surface, and chemical reactions, which can be used for the development of a chemical mechanical polishing (CMP) simulator, the optimization of process parameters, and the design of the next generation of CMP machines. Jin and Zhang analytically proposed a statistical model based on the statistical theory and the abrasive material surface contact mechanisms for predicting the material removal in mechanical polishing and considered that the material removal is the sum of the contributions from the two types of abrasive interactions [12]. Based on the elastic-plastic micro-contact mechanics and abrasive wear theory, Chen et al. established a novel model for material removal rate with consideration of the abrasive particle deformation in chemical mechanical polishing and investigated the effects of particle deformation [13]. Wang et al. presented a model for predicting the material removal depth of the workpiece surface with the stone polishing [14]. In this

model, the effect of the grain size on material removal depth was considered. Lin developed an analytical model based on the micro-contact elastic mechanics, micro-contact elastic-plastic mechanics, and abrasive wear theory for the material removal rate during specimen polishing [15]. This modeling method is relative complex due to using the probability statistics and the contact mechanics, etc. There are some other parameters such as physical property of workpiece, grit, distribution function of grain, geometry of grain, etc., besides the tool speed, the feed rate, and the polishing pressure. The main difficulty in using this model is in obtaining those parameters. In these years, the research results from the grinding wheel topography models have also provided great help for further studying the material removal model.

The third approach is based on Archard equation [16–18]. Fan et al. built a model of material removal profile in free abrasive polishing, which is proposed to facilitate more accurate polishing by analyzing the contact among polishing pad, abrasive grain, and workpiece surface in the micro level etc. [16]. Feng et al. built a model of material removal depth distribution along the vertical direction of feed rate and performed the experiments to evaluate the model of calculating material removal profile. It is used for the automatic precision polishing of curved surfaces using an elastic disk mounted on the spindle of a five-axis machining centre [17]. Chen et al. developed a quantitative model to estimate the material removal of polycrystalline diamond composites by dynamic friction polishing [18]. This model accounts for the contributions from the constitutive characteristics and thermal properties of the materials and the key polishing parameters. In this method, the material removal process is regarded as wear process, and a friction coefficient should be reasonably chosen according to specific polishing pattern.

The fourth approach is based on the experiment investigation [19–22]. In this approach, models are generally developed relating the machining variables with the material removal rate. Zeng and Blunt built a material removal rate based on experiments which were carried out on a bonnet polishing machine in order to investigate the effects of process parameters, including process angle, head speed, tool offset, and tool pressure, on material removal rate [19]. Pan et al. deduced an empirical material removal rate expression based on the experimental data about copper chemical mechanical polishing [21]. Klocke and Zunke finished many polishing experiments and revealed the influence of pressure and relative velocity on the material removal rate in polishing of silicon-based advanced ceramics [22]. This material removal model is restricted to specific polishing equipment, so it needs to be amended when some machining conditions change.

The mould surface polishing is a complex material removal process. The interaction nature is statistical due to the random distributions of sizes and the irregular geometries of the surface asperities and abrasive grains. For the polishing system used for finishing large mould, factors affecting the material removal depth include the polishing force, speed, polishing pad, workpiece, and slurry characteristics. So, considering the grain protrusion height distribution in abrasive tool surface and the material removal mechanism in process of modeling material removal is the development trend in the future. However, the material removal models suitable for large mould free-form surface polishing with varying curvature slightly have not been reported so far. In this study, aiming at large mould polishing, the material removal depth model is developed on the basis of statistical theory and the abrasive material surface contact mechanics. This paper presents the material removal profile model in detail and analyzes the effect laws of process parameters on the material removal profile shape when the workpiece surface was polished by using coated abrasives. These research results can provide theoretical foundation for planning polishing path and controlling process parameters to achieve the uniform material removal purpose.

2 Modeling material removal profile

2.1 Material removal depth

The action type between the polishing tool and workpiece in large mould polishing is shown in Fig. 1. The coated abrasives are suitable for polishing large mould free-form surface with varying curvature slightly. The contact between the coated abrasives and workpiece surface is regarded as the plane contact. So, the pressure in the contact region is equal approximately in this case. The coated abrasives motion diagram of Fig. 1 is given in Fig. 2.

Firstly, unit removal depth (linear removal intensity) is defined as the material removal depth of per unit contact length along the polishing path in the contact region between the tool and the workpiece, which is equivalent to the liner wear intensity in sense. The linear removal depth is calculated as follows [14]:

$$D_l = dz/dy = (N_0 v \tan(\alpha/2)/v_a)\left(\int_{3\sigma-m+\delta_{\max}}^{3\sigma} k^2 (h-(3\sigma-m))^2 f(h) dh \right) \quad (1)$$

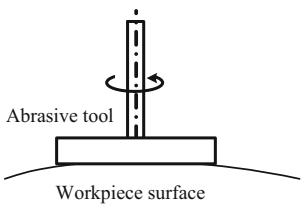

Fig. 1 The action type of the abrasive tool and workpiece

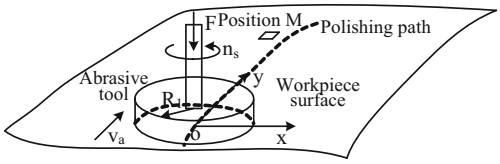

Fig. 2 Polishing process diagram

where D_l is linear removal intensity, namely the material removal depth of per unit contact length along the polishing path, dz is the material removal depth at infinitesimal M during the time interval dt, N_0 is the number of the abrasive grains per unit area, v is the relative velocity between the tool and the workpiece, α is the apical angle of the abrasive grain, v_a is feed rate, σ is the standard deviation of Gaussian distribution, $\delta_{\max}$ is maximum overlap of elastic contact, m is the indentation depth of the abrasive grain, h is the abrasive grain protrusion height, and k is the ratio of the cutting depth to the indentation depth; Atkins and Liu developed the range of k for the various critical attack angles [23]. Calculations about the parameters N_0, α, σ, m, and $\delta_{\max}$ are given in the appendix of this paper.

The removal depth of unit time refers to the workpiece surface removal depth of unit time along polishing path. According to the analysis above, the relation between the contact length per unit time and feed rate is expressed as follows:

$$dy = v_a dt \tag{2}$$

where d_y is the contact length, v_a is the feed rate, and dt is the unit time.

Substituting Eq. (2) into Eq. (1), and defining D_t=dz/dt, then Eq. (1) may be rewritten as follows:

$$D_t = dz/dt = (N_0 v \tan(\alpha/2))\left(\int_{3\sigma-m+\delta_{\max}}^{3\sigma} k^2(h-(3\sigma-m))^2 f(h)dh \right) \tag{3}$$

where D_t is the material removal depth of unit time. The relation between D_l and D_t is expressed as follows:

$$D_t = D_l v_a \tag{4}$$

In the polishing process, the material removal depth for one unit contact length D_l (linear removal intensity) can be calculated by using Eq. (1) when pressure, abrasive material, tool speed, feed rate, and other parameters are known. The material removal depth for a certain position may be obtained by integrating D_l along polishing path, i.e.

$$z_M = \int_{L_1}^{L_2} D_l dL \tag{5}$$

where Z_M is the material removal depth for position M, L_1 is the start point of polishing contact path, and L_2 is the end point of polishing contact path.

Using the material removal depth function of unit time, the material removal depth is expressed as follows:

$$Z_M = \int_{t_1}^{t_2} D_t dt \tag{6}$$

where t_1 is the start time of polishing contact path and t_2 is the end time of polishing contact path.

2.2 Material removal profile

2.2.1 Polishing along straight line

A circle tool of radius R_1, with rotation speed v_s and feed rate v_a moves along straight line paralleling to y axis under a certain polishing pressure. The motion analysis diagram is given in Fig. 3a. The polishing contact trajectory is segment L_1L_2 for passing position M on the workpiece surface, so the material removal depth is

$$Z_M = \int_{y_1}^{y_2} D_l dy \tag{7}$$

where y_1 is the start point of polishing contact path and y_2 is the end point of polishing contact path.

In Fig. 3a, the coordinates of L_1 point and L_2 point are $\left(x, \sqrt{{R_1}^2-x^2}\right)$ and $\left(x, -\sqrt{{R_1}^2-x^2}\right)$, respectively. The speed v of every position in the contact region between abrasive tool and workpiece surface is varied along segment L_1L_2. For example, the speed of A point in Fig. 3a is expressed as follows:

$$v = \sqrt{v_s^2 + v_a^2 + 2v_s v_a \cos\theta} \tag{8}$$

where θ is the angle between tool rotation speed direction and feed rate direction, v_s is the tool rotation speed of A point and

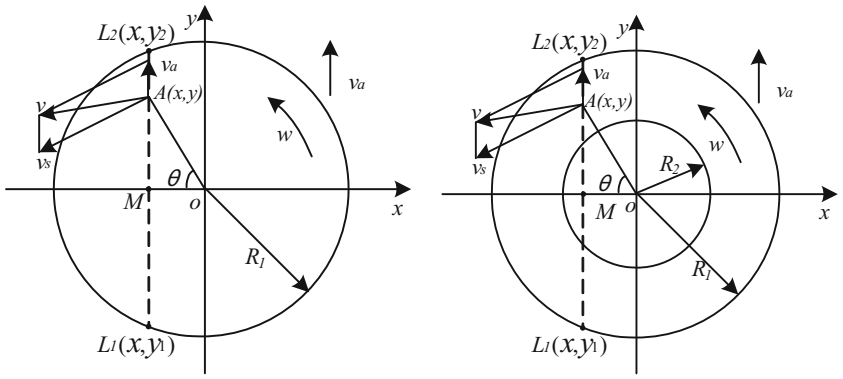

(a) The circular abrasive tool (b) The annular abrasive tool

Fig. 3 Motion analysis diagram along line movement. **a** The circular abrasive tool and **b** the annular abrasive tool

equal to $\omega\sqrt{x^2+y^2}$, among ω is angular velocity of tool rotation and equal to $2\pi n_s$, n_s is also angular velocity of tool rotation, i.e. rotation per minute.

Because of $v_s>>v_a$, the velocity of every point along polishing contact trajectory (e.g. segment L_1L_2) is

$$v\approx v_s=\omega\sqrt{x^2+y^2} \tag{9}$$

So, Eq. (7) is simplified as

$$Z(x)=2\int_0^{\sqrt{{R_1}^2-x^2}} D_l dy \tag{10}$$

Substituting Eq. (9) into Eq. (1), then substituting Eq. (1) into Eq. (10), with the result that

$$Z(x)=2\int_0^{\sqrt{{R_1}^2-x^2}} D_l dy=(2N_0\tan(\alpha/2)/v_a)\left(\int_{3\sigma-m}^{3\sigma} k^2(h-(3\sigma-m))^2 f(h)dh\right)\left(\int_0^{\sqrt{R_1^2-x^2}} \omega\sqrt{x^2+y^2}dy\right) \tag{11}$$

Since the velocity of center point for circular abrasive tool is equal to zero, the annular abrasive tools are usually used. For motion analysis diagram of the annular abrasive tool, as shown in Fig. 3b, the material removal depth is modeled as follows:

When $-R_1\le x\le -R_2$ and $R_2\le x\le R_1$, the material removal depth is

$$Z(x)=2\int_0^{\sqrt{{R_1}^2-x^2}} D_l dy=(2N_0\tan(\alpha/2)/v_a)\left(\int_{3\sigma-m}^{3\sigma} k^2(h-(3\sigma-m))^2 f(h)dh\right)\left(\int_0^{\sqrt{R_1^2-x^2}} \omega\sqrt{x^2+y^2}dy\right) \tag{12}$$

When $-R_2\le x\le R_2$, the material removal depth is

$$Z(x)=2\left(\int_0^{\sqrt{R_1^2-x^2}} D_l dy-\int_0^{\sqrt{R_2^2-x^2}} D_l dy\right)=(2N_0\tan(\alpha/2)/v_a)\left(\int_{3\sigma-m}^{3\sigma} k^2(h-(3\sigma-m))^2 f(h)dh\right)\left(\int_{\sqrt{R_2^2-x^2}}^{\sqrt{R_1^2-x^2}} \omega\sqrt{x^2+y^2}dy\right) \tag{13}$$

2.2.2 Polishing along curve

The abrasive tool often moves on the workpiece surface along curve. On the assumption that the curvature radius of curve is R_0 and the angle velocity of tool rotation is ω_{o1} along center point O_1, as given in Fig. 4a, if the contact trajectory is circular arc L_1L_2 for passing a certain position M on the workpiece surface, the material removal depth is

$$Z_M=\int_{t_1}^{t_2} D_t dt \tag{14}$$

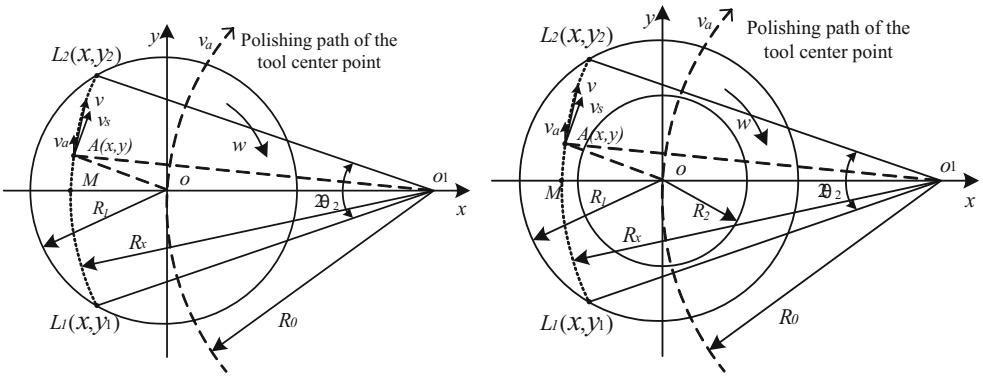

(a) The circular abrasive tool (b) The annular abrasive tool

Fig. 4 Motion analysis diagram along curve movement. **a** The circular abrasive tool and **b** the annular abrasive tool

According to $\theta=\omega_{o1}t$, $d\theta=\omega_{o1}dt$ can be obtained. The rotation linear velocity of the abrasive tool are $v_s=\omega\cdot OA$ and $v_a=\omega_{o1}(R_0-x)$ at point A, respectively. Because of $v_s>>v_a$, the velocity of every point along polishing contact trajectory (e.g. circular arc L_1L_2) is written as

$$v\approx v_s=\omega\sqrt{R_0^2+(R_0-x)^2-2R_0(R_0-x)\cos\theta} \tag{15}$$

For Eq. (14), it can be expressed as

$$Z(x)=\int_{t_1}^{t_2}D_t dt=2\int_0^{\theta_2}D_t d\theta/\omega_{o1} \tag{16}$$

Substituting Eq. (15) into Eq. (3), then substituting Eq. (3) into Eq. (16), and solving for Z_M yields

$$\begin{aligned}Z(x)&=2\left(\int_0^{\theta_2}D_t d\theta\right)\Big/\omega_{o1}\\&=(2N_0\tan(\alpha/2)/v_a)\left(\int_{3\sigma-m}^{3\sigma}k^2(h-(3\sigma-m))^2f(h)dh\right)\\&\quad\left(\int_0^{\theta_2}\omega(R_0-x)\sqrt{R_0^2+(R_0-x)^2-2R_0(R_0-x)\cos\theta}d\theta\right)\end{aligned} \tag{17}$$

where θ_2 is the angle of the end position of polishing contact trajectory, which can be obtained from the expression

$$\theta_2=arc\cos\frac{R_0^2+(R_0-x)^2-R_1^2}{2R_0(R_0-x)} \tag{18}$$

Similarly, for the annular abrasive tool, when moving along curve, as shown in Fig. 4b, the material removal depth is modeled as follows:

When $-R_1\le x\le -R_2$ and $R_2\le x\le R_1$, the material removal depth is

$$\begin{aligned}Z(x)&=2\left(\int_0^{\theta_2}D_t d\theta\right)\Big/\omega_{o1}\\&=(2N_0\tan(\alpha/2)/v_a)\left(\int_{3\sigma-m}^{3\sigma}k^2(h-(3\sigma-m))^2f(h)dh\right)\\&\quad\left(\int_0^{\theta_2}\omega(R_0-x)\sqrt{R_0^2+(R_0-x)^2-2R_0(R_0-x)\cos\theta}d\theta\right)\end{aligned} \tag{19}$$

When $-R_2\le x\le R_2$, the material removal depth is

$$\begin{aligned}Z(x)&=2\left(\int_0^{\theta_2}D_t d\theta-\int_0^{\theta_4}D_t d\theta\right)\Big/\omega_{o1}\\&=(2N_0\tan(\alpha/2)/v_a)\left(\int_{3\sigma-m}^{3\sigma}k^2(h-(3\sigma-m))^2f(h)dh\right)\\&\quad\left(\int_{\theta_4}^{\theta_2}\omega(R_0-x)\sqrt{R_0^2+(R_0-x)^2-2R_0(R_0-x)\cos\theta}d\theta\right)\end{aligned} \tag{20}$$

where θ_4 is the angle of the start position of polishing contact trajectory, which can be obtained from the expression

$$\theta_4=arc\cos\frac{R_0^2+(R_0-x)^2-R_2^2}{2R_0(R_0-x)} \tag{21}$$

The model established above can be used for predicting material removal profile under different machining conditions when the large mould free-form surface with varying curvature slightly is polished by using the coated abrasives. The advantages of this model are that it not only contains the machining parameters (polishing force, feed rate, tool rotation speed, etc.) but also considers the effects of the mechanical

properties of the workpiece (material hardness) and abrasive tool parameters (grit, the circular abrasive tool, and the annular abrasive).

3 Simulation and experiment verification

3.1 Simulation

The effect laws of some process parameters on the removal depth were simulated and analyzed when polishing path is a straight line. The adopted simulation parameters are listed in the Table 1. The material removal depth profile curves with various tool rotation speeds are shown in Fig. 5 (material AISI 1045, circle abrasive tool, polishing force 20 N, feed rate 200 mm/min). The material removal depth profile curves with various feed rates are shown in Fig. 6 (material AISI 1045, circle abrasive tool, polishing force 20 N, tool speed 500 r/min). The material removal depth profile curves with various polishing forces are shown in Fig. 7 (material ductile iron, annular abrasive tool, tool speed 500 r/min, feed rate 200 mm/min). The material removal depth profile curves with various inner circle radii are shown in Fig. 8 (material ductile iron, polishing force 25 N (R_2=7.5 um), 20 N (R_2=12.5 um), 15 N (R_2=17.5 um), tool speed 500 r/min, feed rate 200 mm/min).

3.2 Experiment verification

Many polishing experiments were carried out. A kind of coated abrasives used in the experiment is given in Fig. 9. The plane workpieces were polished by using annular abrasive tools moving along the straight line. Workpiece material are AISI 1045 and ductile iron, respectively. The workpiece surface prior to polishing is milled. Milling process conditions for AISI 1045 are the following: ball-end mill (material high speed steel, radius 6 mm), radial milling distance 0.5 mm, spindle rotation speed 1,000 r/min, milling velocity 100 mm/min, axial milling depth 0.9 mm. Milling process conditions for ductile iron are the following: ball-end mill (material high speed steel, radius 10 mm), radial milling distance 0.65 mm, spindle rotation speed 500 r/min, milling velocity 200 mm/min, axial milling depth 0.8 mm. Workpieces (ductile iron) before and after polishing are presented in Fig. 10. There is clear milling mark in the workpiece surface before polishing in the Fig. 10a, which is produced by the ball milling cutter. There are obviously two polishing zones, as shown in Fig. 10b, in which the surface material have already been removed uniformly and there is no milling mark except for polishing marginal areas, workpiece surface becomes smooth, and surface roughness decreases. The experiment conditions are given in Table 2. The simulation and experiment results of the material removal depth with various polishing parameters are shown in Fig. 11 (no. 1 in the Table 2, outer radius 25 mm, inner radius 12.5 mm) and Fig. 12 (no. 5 in the Table 2, outer radius 45 mm, inner radius 27.5 mm).

Table 1 Simulation parameters

Item	Content
Abrasive tool	Abrasive material: chrome corundum, grit: $150^{\#}$(75–106 um), $E_1=4\times10^5$ MPa, $v_1=0.3$, circle abrasive tool and annular abrasive tool, R_1=25 mm, R_2=12.5 mm
Workpiece	Material 1: AISI 1045 $E_2=2.06\times10^5$ MPa, $v_2=0.3$ Material 2: ductile iron $E_2=1.54\times10^5$ MPa, $v_2=0.3$
Other parameters	F=10, 15, 20, 25 N; k=0.04; n_s=500, 1,000 r/min; v_a=200, 400 mm/min; R_2=7.5, 12.5, 17.5 mm

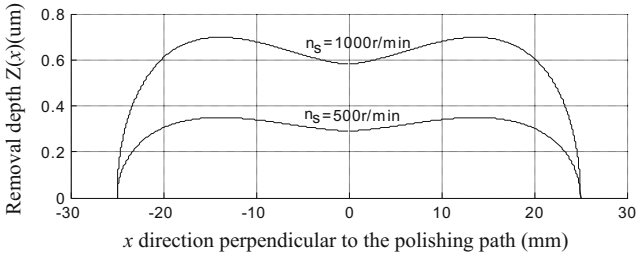

Fig. 5 The removal profile of various tool rotation speeds

4 Discussion

It can be seen from Figs. 5 and 6 that the material removal depth is directly proportional to the tool rotation speed and inversely proportional to the feed rate and the material removal depth at center point is smaller than that of other positions except for the fringe region. The increase in the value of tool rotation speed raises the number of the abrasive grains participating in the cutting on workpiece surface; as a result, the material removal depth increases rapidly. The increase in the value of feed rate decreases the number of the abrasive grains participating in the cutting on workpiece surface, so the material removal depth decreases. Figure 7 shows the effects of

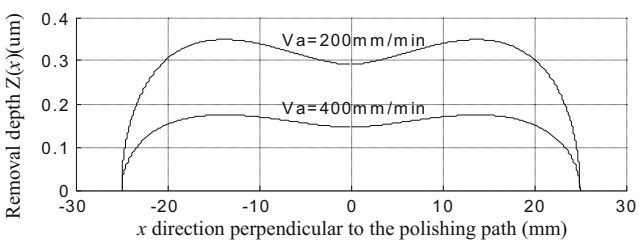

Fig. 6 The removal profile of various feed rates

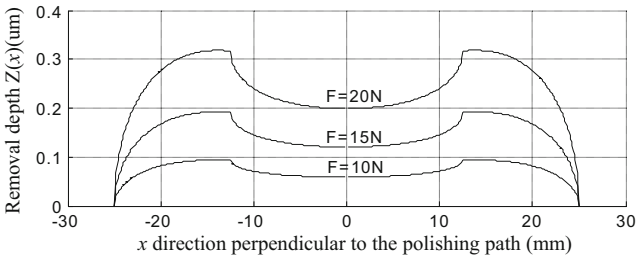

Fig. 7 The removal profile of various polishing forces

Fig. 9 Coated abrasives

the polishing force on the removal depth. It shows that the material removal depth increases with increasing polishing force. In fact, the material removal depth increases with the increase of pressure in certain range, and the material removal depth ceases to increase with any further increase in the pressure. For example, for circle abrasive tool, the material removal depth at center point is smaller than that of other positions except for fringe region. The material removal depth reaches high far from circle center position about 15 mm when the abrasive tool radius is equal to 25 mm, which is a result of comprehensive effect of various factors at this position, such as polishing pressure, feed rate, tool rotation speed, and participating in numbers of abrasive grains. Figure 8 shows the effect of the inner circle radius on the removal depth. For the annular abrasive tool, the removal profile becomes farther non-uniform with increasing inner circle radius, and the material removal depth at center point is also smaller than that of other positions except for fringe region, which are produced because of the effective contact area and rotation speed for various position contacted. For example, the effective contact areas at center region decrease with increase of inner circle radius.

For theory simulation curves in Figs. 11 and 12, the material removal depth at center position is smaller than that of other positions except for fringe region curves. However, for experiment curves in Figs. 11 and 12, the material removal depth is relatively uniform on the whole and is equal to theory calculation result of middle position. The reason is that the contact pressure of every position between the abrasive tool and workpiece surface is assumed to be equal in theory modeling, but local contact pressure is not equal due to different material removal depth in practice. The material removal amount of workpiece surface having high polishing pressure is more than that of others, which results that the uniform removal profile is achieved at last. There are obvious changes about removal depth at both end positions in Figs. 11 and 12. The width of fringe region is approximately equal to 2 mm, which also provides significant foundation for determining polishing spacing as planning polishing path. In addition, Table 2 gives material removal depth of theory and experiment at center position for each experiment, respectively. Based from those analyses above, it can be concluded that the experiment results are in agreement with theory simulation results by and large. So, the material removal depth can be calculated by using this model presented in this study.

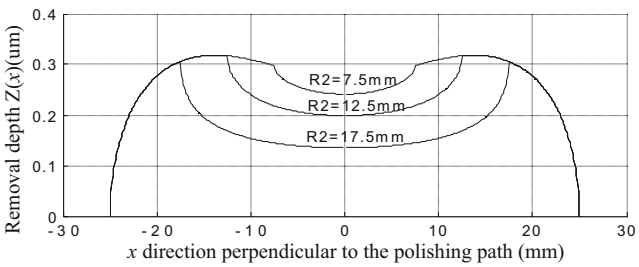

Fig. 8 The removal profile of various internal radii

5 Conclusions

(1) A material removal profile model of workpiece surface polished by coated abrasives was successfully developed. This model is based on the probability statistics, the contact plastic mechanics, and the abrasive cutting theory and suitable for large mould free-form surface with varying curvature slightly. The material removal depth profiles were investigated when polishing paths

(a) Workpiece prior to polishing (b) Workpiece polished

Fig. 10 The workpiece surface. **a** Workpiece prior to polishing and **b** workpiece polished

Table 2 Experiment and simulation results

No.	Material	Grit	Polishing force (N)	Tool speed (r/min)	Feed rate (mm/min)	Center position (um)	
						Theory	Experiment
1	AISI 1045	150#	20	500	30	3.802	3.928
2	AISI 1045	150#	40	500	90	3.627	3.852
3	AISI 1045	150#	20	1,000	90	2.534	2.361
4	AISI 1045	150#	40	1,000	200	1.632	1.564
5	Ductile iron	120#	40	1,000	200	0.613	0.673
6	Ductile iron	120#	40	500	90	0.681	0.730

are straight line and curve, respectively. The factors affecting the material removal depth include the mechanical properties of the workpiece and tool, the polishing tool specifications (grain size, etc.), and polishing conditions (pressure, feed rate, tool rotation speed, etc.).

(2) The effect laws of the process parameters on material removal depth were obtained. The depth of material removal profile increases with the increase of the tool rotation speed, and the depth of material removal profile decreases with the increase of feed rate. For the coated abrasives given in this paper, the material removal depth increases when polishing pressure increases within a certain range. The more workpiece material hardness is, the less material removal depth is, because the material with greater hardness needs greater pressure at the same indentation depth. When other factors such as polishing pressure remain unchanged, with increasing inner radius of abrasive tool, the material removal depth decreases at inner region of the removal profile, and the material removal depth remain unchanged at annular region of the removal profile.

(3) The material removal profile curves obtained from polishing experiments are relatively uniform on the whole, and material removal depth is equal to that of center region obtained from theory. The width of fringe region is about equal to 2 mm. Comparison between prediction and experimental results provide reasonable quantitative agreement. This model developed in this study predicts quantitatively the material removal depth, which prepares theoretical foundation for achieving good machining quality and high efficiency.

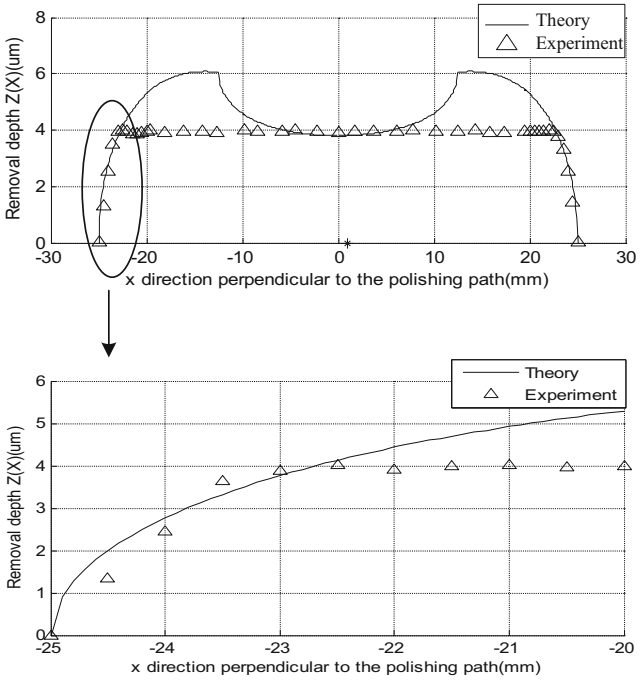

Fig. 11 Theory curves and experiment results (AISI 1045)

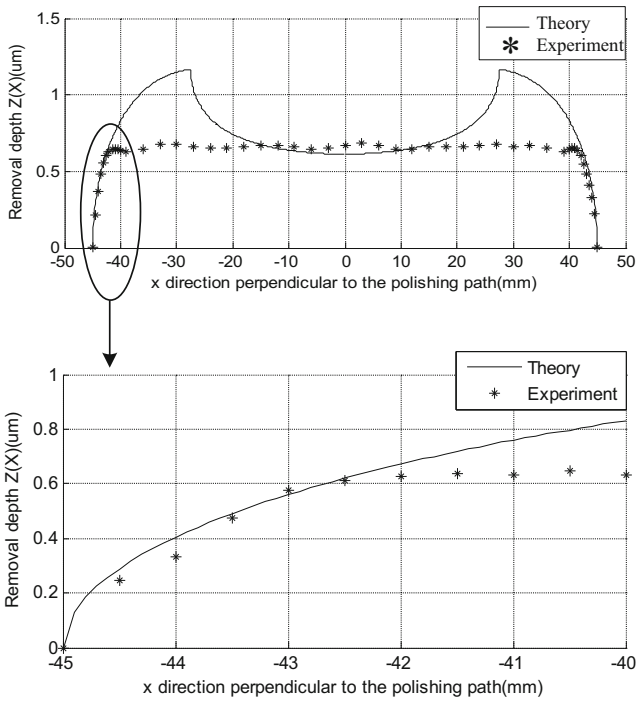

Fig. 12 Theory curves and experiment results (ductile iron)

Acknowledgments This project is supported by National Natural Science Foundation of China (Grant No. 51405196), Natural Science Foundation of Heilongjiang Province (Grant No. E201464), and Department of Education of Heilongjiang Province (Grant No. 12531660).

Appendix

N_0 (The number of the abrasive grains per unit area)

The abrasive grain sizes are determined in terms of the value of grit. The maximum diameter d_{max} and minimum diameter d_{min} of the abrasive grains can be determined when the grit is known. The mean diameter d_m of the abrasive grains is defined by

$$d_m = (d_{\max} + d_{\min})/2 \tag{22}$$

Values of d_{max}, d_{min} for different grain sizes are shown in Table 3.

The number of the abrasive grains per unit area N_0 is given by

$$N_0 = 6 \times V_g/\left(\pi d_m^2\right) \tag{23}$$

where V_g (%) is the grain ratio, V_g=2(31−S), S is structure number of the abrasive tool.

α (Apical angle)

For a single abrasive grain capped with spherical top of radius of curvature R, assume that the shape of the abrasive grain is cone with apical angle α, with an increase of the grain size, both radius R and apical angle α also increase. α of most abrasive grains is between 90° and 120°. Table 4 shows the values of R and α for kinds of the grits.

Table 3 d_{max}, d_{min} for different grain sizes

Grit	d_{max} (×10^{-3} mm)	d_{min} (×10^{-3} mm)
100#	150	125
120#	125	106
150#	106	75
180#	90	63
220#	75	53
W40	40	28

Table 4 R and α for kinds of the grits

Grit	46#	60#	80#	W40	W28
R (×10^{-3} mm)	28	18	13	4	2.7
α	110°	108°	106°	98°	90°

σ (Standard deviation of Gaussian distribution)

d_{max} and d_{min} are very close to the maximum abrasive grain protrusion height and the minimum abrasive grain protrusion height, respectively. Standard deviation of Gaussian distribution σ can be calculated as follows:

$$\sigma = (d_{\max} - d_{\min})/6 \tag{24}$$

$\delta_{\max}$ (Maximum overlap of elastic contact)

The maximum overlap of elastic contact $\delta_{\max}$ can be calculated as

$$\delta_{\max} = \frac{\pi^2 R H_B^2}{16 E^{*2}} \tag{25}$$

where E* is the contact modulus of the abrasive grain and workpiece, given by $\frac{1}{E^*} = \frac{1-\nu_1^2}{E_1} + \frac{1-\nu_2^2}{E_2}$, where E_1 and E_2 are Young's modulus of the abrasive grain and workpiece, ν_1 and ν_2 are Poisson's ratio of the abrasive grain and workpiece, respectively, H_B is the Brinell hardness of the workpiece surface.

m (Indentation depth of the abrasive grain)

Relation between indentation depth of the abrasive grain m and pressure P can be expressed as

$$\begin{aligned} P = F_t + F_{S1} + F_{S2} = {} & \frac{4NE^*\sqrt{R}}{3\sqrt{2\pi}\sigma}\int_{3\sigma-m}^{3\sigma-m+\delta_{\max}} (h-(3\sigma-m))^{\frac{3}{2}} e^{-\frac{h^2}{2\sigma^2}} dh \\ & + \frac{N\pi H_B}{2\sqrt{2\pi}\sigma}\int_{3\sigma-m+\delta_{\max}}^{3\sigma-m+R} (h-(3\sigma-m))(2R+3\sigma-m-h) e^{-\frac{h^2}{2\sigma^2}} dh \\ & + \frac{N\pi\left(\tan\left(\alpha/2\right)\right)^2 H_B}{2\sqrt{2\pi}\sigma}\int_{3\sigma-m+R}^{3\sigma} (h-(3\sigma-m))^2 e^{-\frac{h^2}{2\sigma^2}} dh \end{aligned} \tag{26}$$

Using Eq. (26), m can be calculated.

References

1. Yang Z, Chen F, Zhao J, Wu X (2009) A novel vision localization method of automated micro-polishing robot. J Bionic Eng 6(1):46–54
2. Tsai M, Huang J, Kao W (2009) Robotic polishing of precision molds with uniform material removal control. Int J Mach Tools Manuf 49: 885–895
3. Guo HR, Wu YB, Lu D, Fujimoto M, Nomura M (2014) Effects of pressure and shear stress on material removal rate in ultra-fine polishing of optical glass with magnetic compound fluid slurry. J Mater Process Technol 214(11):2759–2769
4. Dong ZC, Cheng HB (2014) Study on removal mechanism and removal characters for SiC and fused silica by fixed abrasive diamond pellets. Int J Mach Tools Manuf 85:1–13
5. Guo J, Suzuki H, Higuchi T (2013) Development of micro polishing system using a magnetostrictive vibrating polisher. Precis Eng 37:81–87
6. Liu XY, Liu YL, Liang Y, Zhao ZW, Gao BH (2012) Kinetics model incorporating both the chemical and mechanical effects on material removal for copper chemical mechanical polishing. Microelectron Eng 91:19–23
7. Lin ZC, Huang WS, Tsai JS (2012) A study of material removal amount of sapphire wafer in application of chemical mechanical polishing with different polishing pads. J Mech Sci Technol 26(8): 2353–2364
8. Cheung CF, Kong LB, Ho LT, To S (2011) Modeling and simulation of structure surface generation using computer controlled ultra-precision polishing. Precis Eng 35:574–590
9. Kim S, Saka N, Chun JH (2014) The effect of pad-asperity curvature on material removal rate in chemical-mechanical polishing. Procedia CIRP 14:42–47
10. Lin ZC, Wang RY (2014) Abrasive removal depth for polishing a sapphire wafer by a cross-patterned polishing pad with different abrasive particle sizes. Int J Adv Manuf Technol 74(1–4):25–36
11. Lee HS, Jeong HD, Dornfeld DA (2013) Semi-empirical material removal rate distribution model for SiO2 chemical mechanical polishing (CMP) processes. Precis Eng 37:483–490
12. Jin XL, Zhang LC (2012) A statistical model for material removal prediction in polishing. Wear 274–275:203–211
13. Chen XC, Zhao YW, Wang YG (2012) Modeling the effects of particle deformation in chemical mechanical polishing. Appl Surf Sci 258(22):8469–8474
14. Wang GL, Wang YQ, Xu ZX (2009) Modeling and analysis of the material removal depth for stone polishing. J Mater Process Technol 209:2453–2463
15. Lin TR (2007) An analytical model of the material removal rate between elastic and elastic-plastic deformation for a polishing process. Int J Adv Manuf Technol 32(7–8):675–681
16. Fan C, Zhao J, Zhang L, Wong YS, Hong GS, Zhou WS (2014) Modeling and analysis of the material removal profile for free abrasive polishing with sub-aperture pad. J Mater Process Technol 214: 285–294
17. Feng DY, Sun YW, Du HP (2014) Investigations on the automatic precision polishing of curved surfaces using a five-axis machining centre. Int J Adv Manuf Technol 72(9–12):1625–1637
18. Chen Y, Nguyen T, Zhang LC (2009) Polishing of polycrystalline diamond by the technique of dynamic friction—Part 5: quantitative analysis of material removal. Int J Mach Tools Manuf 49:515–520
19. Zeng SY, Blunt L (2014) Experimental investigation and analytical modelling of the effects of process parameters on material removal rate for bonnet polishing of cobalt chrome alloy. Precis Eng 38:348–355
20. Zeng S, Blunt L (2014) An experimental study on the correlation of polishing force and material removal for bonnet polishing of cobalt chrome alloy. Int J Adv Manuf Technol 73(1–4):185–193
21. Pan GS, Wang N, Gong H, Liu Y (2012) An empirical approach to explain the material removal rate for copper chemical mechanical polishing. Tribol Int 47:142–144
22. Klocke F, Zunke R (2009) Removal mechanisms in polishing of silicon based advanced ceramics. CIRP Annals-Manufacturing Technology 58:491–494
23. Atkins AG, Liu JH (2007) Toughness and the transition between cutting and rubbing in abrasive contacts. Wear 262: 146–159